

Cite this: *J. Mater. Chem. A*, 2023, 11, 2996

Modulation of double-network hydrogels via seeding calcium carbonate microparticles for the engineering of ultrasensitive wearable sensors†

Xiaohui Zhang,^a Huimin Geng,^a Xunhui Zhang,^a Yaqing Liu,^{ID}^a Jingcheng Hao^{ID}^{*a} and Jiwei Cui^{ID}^{*ab}

Double-network (DN) hydrogels with high strength and toughness have shown their potential for applications in materials science and biomedical engineering. Biocompatible sodium alginate (SA)/polyacrylamide (PAM) hydrogels are a promising class of DN hydrogels, which are typically cross-linked with calcium ions (Ca²⁺). However, the use of calcium salts typically induces structural inhomogeneity and reduces the mechanical properties of the resultant hydrogels, which limit their application in tissue scaffolds, actuators, and wearable devices. Herein, we fabricate a homogeneous polymer DN hydrogel by pre-seeding calcium carbonate (CaCO₃) microparticles into SA/PAM hydrogels, followed by the triggered release of Ca²⁺ from the microparticles in acidic solution. The acid-triggered cross-linking generates sacrificial ionic bonds capable of dissipating energy, which endows the Ca²⁺/SA/PAM DN hydrogels with high tensile strength (0.85 MPa), stretchability (1850%), and fracture toughness (6.4 MJ m⁻³). These properties can be easily adjusted by controlling the trigger time as well as the concentration of the CaCO₃ microparticles. In addition, the Ca²⁺/SA/PAM DN hydrogel exhibits high strain sensitivity with a gauge factor of ~8.9, a wide strain detection range (0.03–1800%), and excellent durability (500 cycles at a strain of 50%), which can be used as a strain sensor to monitor human motions with a fast response (~0.02 s). Furthermore, the Ca²⁺/SA/PAM DN hydrogel as a sensor can monitor the pain signal induced by an *in situ* cascade reaction at a wound site in a diabetic rat model. This study provides a controllable strategy to engineer stretchable and tough DN hydrogels for potential applications in flexible devices.

Received 7th October 2022
Accepted 11th January 2023

DOI: 10.1039/d2ta07834a

rsc.li/materials-a

1. Introduction

Hydrogels are unique soft materials with three-dimensional network structures capable of absorbing and retaining large amounts of aqueous solutions.^{1–4} They are widely used in various fields, including tissue engineering,^{5–7} sensing,^{8–11} actuation,^{12–14} soft machines,^{15–17} and flexible electronics.^{18–21} Structural inhomogeneity and the related inefficient energy dissipation result in low mechanical strength of hydrogels and limit their applications. Thus, a series of topological hydrogels,²² nanocomposite hydrogels,^{23–25} macromolecular microsphere composite hydrogels,^{26,27} polyampholyte hydrogels,^{28–30} and double-network (DN)

hydrogels^{31–34} have been developed to increase the mechanical strength and homogeneity of hydrogels. DN hydrogels combine noncovalently (*e.g.*, ionic bonds, hydrogen bonds, hydrophobic interactions, host–guest interactions) and covalently (*e.g.*, covalent bonds) cross-linked networks and can effectively improve the mechanical properties of hydrogels.³⁵ That is, physically cross-linked networks can contribute sacrificial bonds to achieve energy dissipation while stretching, while chemically cross-linked networks endow the hydrogel with sufficient toughness.^{27,32}

Sodium alginate (SA) is a natural polysaccharide and has been widely used for tissue engineering, pharmaceuticals, food products, and textiles due to its good processability with ionic cross-linking, stability and chelation as well as excellent biocompatibility and biodegradability.^{9,36} In addition, SA can be used to prepare ionically cross-linked hydrogels with Ca²⁺, which have been widely used to form DN hydrogels in combination with polymerized polyacrylamide (PAM).^{9,10,32} For example, Suo and co-workers reported an ionically and covalently cross-linked DN hydrogel composed of CaSO₄-alginate and PAM that displayed high extensibility and toughness.³⁷ However, the tensile strength of DN hydrogels was only 160 kPa, which could be attributed to the low solubility of CaSO₄ and therefore caused the insufficient cross-linking of hydrogel networks (Scheme 1a). Alternatively, SA/

^aKey Laboratory of Colloid and Interface Chemistry of the Ministry of Education, School of Chemistry and Chemical Engineering, Shandong University, Jinan, Shandong 250100, China. E-mail: jhao@sdu.edu.cn; jwcui@sdu.edu.cn

^bState Key Laboratory of Microbial Technology, Shandong University, Qingdao, Shandong 266237, China

† Electronic supplementary information (ESI) available: SEM images and photographs of hydrogels; loading–unloading tests, recovery ratios and dissipated energies of Ca²⁺/SA/PAM DN hydrogels; electrical resistance signals from the elbow and wrist; photographs, TEM and zeta potential of MS and MS/GOx@TA/Fe²⁺ NPs; UV-vis absorption spectra of NPs; summary of recent hydrogel-based flexible sensors. See DOI: <https://doi.org/10.1039/d2ta07834a>

PAM hydrogels can be cross-linked by soluble multivalent cations (*e.g.*, Ca^{2+} , Sr^{2+} , Ba^{2+} , Zn^{2+} , Al^{3+} , and Fe^{3+}) in solutions to improve the mechanical properties of DN hydrogels.³⁸ However, it is easy to form a dense shell on the surface of the hydrogels that prevents the permeation of cations into the interior of the hydrogels (Scheme 1b).^{39,40} As a result, DN hydrogels exhibit non-homogeneous cation distribution, which significantly influences the improvement of the mechanical strength.⁴⁰ Therefore, it is desirable to improve the homogeneity of cation distribution in DN hydrogels to enhance their strength.

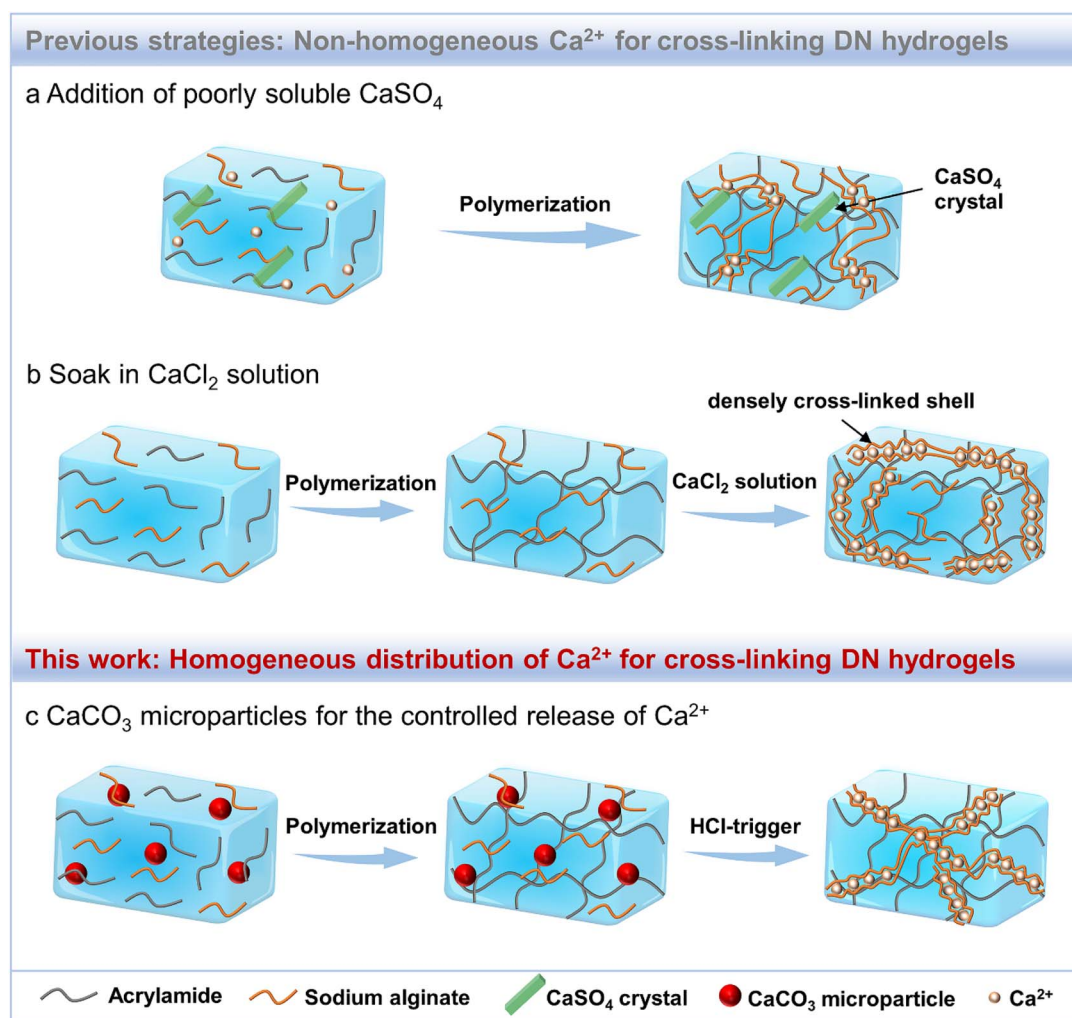
In this study, we report a facile strategy to fabricate ultra-stretchable Ca^{2+} /SA/PAM DN hydrogels *via* uniform distribution of Ca^{2+} for cross-linking of SA. CaCO_3 microparticles are pre-seeded into SA/PAM (denoted as CaCO_3 /SA/PAM) hydrogels and acid (*i.e.*, hydrochloric acid, HCl) can trigger the homogeneous release and distribution of Ca^{2+} to result in tough Ca^{2+} /SA/PAM DN hydrogels (Scheme 1c). The resultant DN hydrogels exhibit higher tensile strength (0.85 MPa), fracture toughness (6.4 MJ m^{-3}), and anti-fatigue properties than those of PAM hydrogels, SA/PAM hydrogels, and CaCO_3 /SA/PAM composite hydrogels. As a result, the Ca^{2+} /SA PAM DN

hydrogels exhibit a wide strain sensing range (0.03–1800%), fast response rate ($\sim 0.02 \text{ s}$), high sensitivity with a gauge factor (GF, ~ 8.9) and repeatability (500 cycles at a strain of 50%). Furthermore, Ca^{2+} /SA/PAM DN hydrogels demonstrate high strain sensitivity in monitoring and distinguishing different motions and physiological signals as wearable strain sensors. The reported strategy of pre-seeding CaCO_3 microparticles and triggering the release of Ca^{2+} provides a unique opportunity to design and fabricate DN hydrogels with high mechanical strength for a wide range of applications (*e.g.*, artificial flexible electronics, wearable devices, and soft robotics).

2. Results and discussion

2.1 Preparation and characterization of Ca^{2+} /SA/PAM DN hydrogels

Free radical polymerization was used for the preparation of CaCO_3 /SA/PAM composite hydrogels. Specifically, acrylamide (AM) powder was added to the SA solution and then mixed with CaCO_3 microparticles, followed by polymerization by incubation with a cross-linker (*N,N'*-methylenebisacrylamide, MBAA),



Scheme 1 Schematic illustration of (a and b) non-homogeneous and (c) homogeneous Ca^{2+} cross-linking strategies for the formation of Ca^{2+} /SA/PAM DN hydrogels.

an initiator (ammonium persulfate, APS), and a catalyst (*N,N,N',N'*-tetramethylethylenediamine, TEMED) for 3 h at 50 °C. PAM and SA/PAM hydrogels were prepared similarly in the absence of CaCO₃ microparticles. Porous structures were observed in freeze-dried PAM and SA/PAM hydrogels (Fig. S1 and S2†). Scanning electron microscopy (SEM) images showed the presence of CaCO₃ microparticles with an average particle size of 3.5 μm (Fig. S3†) in CaCO₃/SA/PAM composite hydrogels (Fig. 1a and b). Confocal laser scanning microscopy (CLSM) confirmed the successful incorporation and homogeneous distribution of CaCO₃ microparticles throughout the CaCO₃/SA/PAM composite hydrogels (Fig. 1c), where CaCO₃ microparticles were labelled with fluorescein isothiocyanate-labelled poly(allylamine hydrochloride) (FITC-PAH). In the absence of CaCO₃ microparticles, the SA/PAM hydrogel was transparent before and after HCl treatment (Fig. S4†), while the CaCO₃/SA/PAM composite hydrogel changed from opaque to transparent after HCl treatment due to the formation of Ca²⁺/SA/PAM DN hydrogels (Fig. S5†). The DN hydrogel had a dense fiber network after the dissolution of CaCO₃ microparticles (Fig. 1d and e), indicating the dissolution of CaCO₃ microparticles after HCl treatment. The released Ca²⁺ resulted in the formation of ionic

cross-linking networks (Fig. 1f), which reduced the water absorption ratio due to the presence of double networks in the hydrogels (Fig. S6†). Fourier transform infrared (FTIR) spectroscopy was further used to examine the cross-linking with Ca²⁺ (Fig. S7†). Specifically, the SA powder showed bands at around 3445, 1618, and 1418 cm⁻¹, ascribed to the stretching of -OH, -COO⁻ (asymmetric), and -COO⁻ (symmetric), respectively,⁴¹ while the -COO⁻ stretching bands shifted to a higher wavenumber (1656 cm⁻¹) in Ca²⁺/SA/PAM DN hydrogels due to formation of ionic bonding between Ca²⁺ and -COO⁻ of SA.^{42,43} Moreover, the increase in the Ca²⁺ concentration resulted in a further shift of the -CO stretching bands to a higher wavenumber (1667 cm⁻¹). Energy-dispersive X-ray spectroscopy (EDS) confirmed the uniform distribution of Ca²⁺ throughout the hydrogel (Fig. 1g). These results demonstrate that homogeneous Ca²⁺/SA/PAM DN hydrogels can be prepared by the triggered release of Ca²⁺ from pre-seeded CaCO₃ microparticles.

2.2 Mechanical properties

Mechanical properties of Ca²⁺/SA/PAM DN hydrogels were examined with different deformations. The Ca²⁺/SA/PAM DN

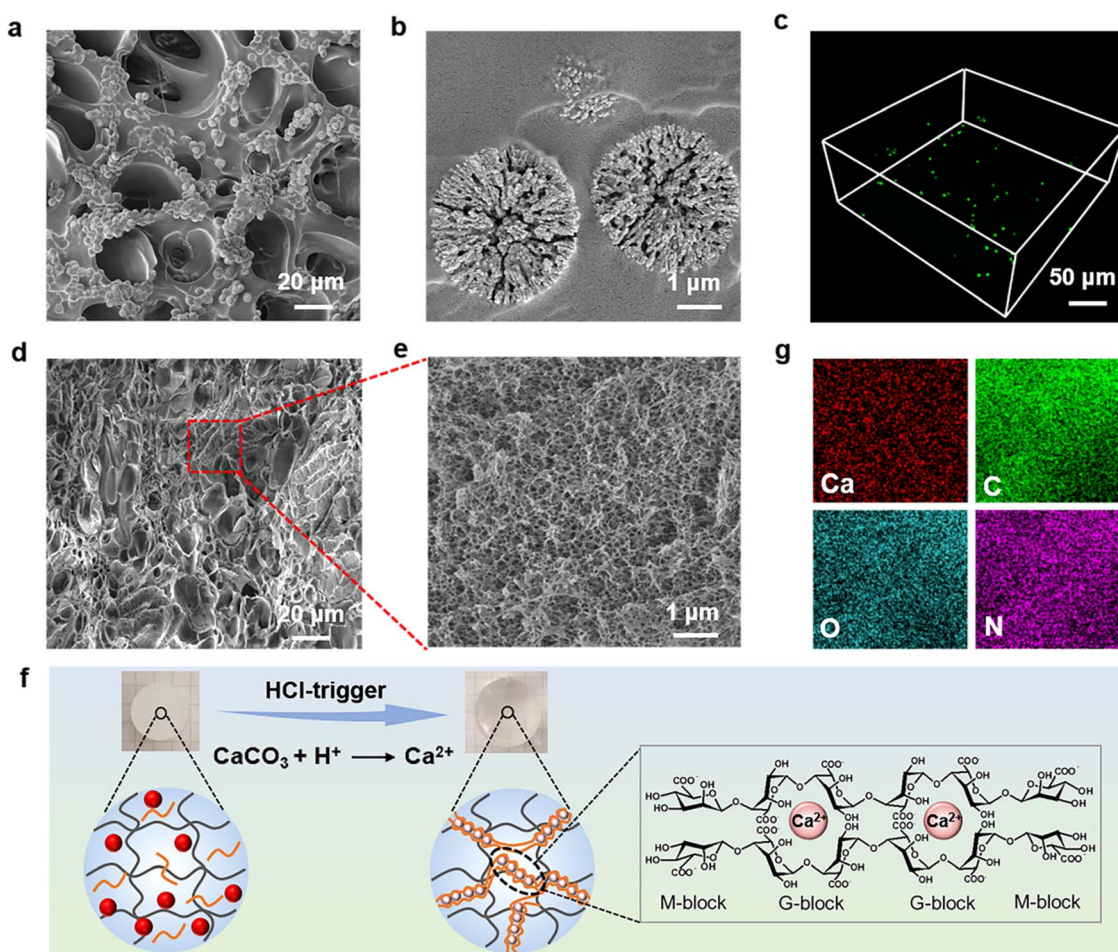


Fig. 1 (a and b) SEM images of the CaCO₃/SA/PAM composite hydrogel. (c) CLSM image of FITC-labelled CaCO₃ microparticles in the CaCO₃/SA/PAM hydrogel. (d and e) SEM images of the Ca²⁺/SA/PAM DN hydrogel after the triggered release of Ca²⁺. (f) Schematic illustration of acid-triggered release of Ca²⁺ and cross-linking of SA networks. (g) EDS mapping of Ca, C, O, and N elements in the Ca²⁺/SA/PAM DN hydrogel.

hydrogel could recover its original shape immediately after pressing and withstand various deformations, including bending, knotting, and stretching with an appreciably high loading ability, demonstrating its excellent flexibility and elasticity. Moreover, a hydrogel strip with a diameter of 5 mm could hold up a 2 kg weight without any damage (Fig. 2a).

Tensile measurements were used to evaluate the mechanical properties of the $\text{Ca}^{2+}/\text{SA}/\text{PAM}$ DN hydrogels. The tensile strength and toughness of the hydrogels could be controlled by the concentration of the incorporated CaCO_3 microparticles (Fig. 2b and c). When the concentration of CaCO_3 microparticles was increased from 1 to 3 mg mL^{-1} , the tensile strength and toughness of hydrogels increased from 0.35 to 0.85 MPa and 1.44 to 6.4 MJ m^{-3} , respectively. However, when the concentration was above 3 mg mL^{-1} , high cross-linking in the hydrogel resulted in brittle networks. At the optimal concentration, the increased cross-linking density and small pores of the hydrogel

could avoid the stress concentration and crack expansion, while the ionic bonds of Ca^{2+} -SA could dissipate the mechanical energy, thereby leading to a high tensile strength. In addition, the tensile strength and toughness of the hydrogels could also be controlled by the HCl incubation time. Along with the increase in the incubation time, both the tensile strength and toughness initially increased and then decreased after 2 h incubation (Fig. 2d and e). The initial increase in tensile strength was attributed to the gradual dissolution of the CaCO_3 microparticles and the release of Ca^{2+} . The maximum tensile strength (0.85 MPa) and toughness (6.4 MJ m^{-3}) were obtained at 2 h, due to the full dissolution of the incorporated CaCO_3 microparticles. Further incubation with HCl caused a significant decrease in the tensile strength of the $\text{Ca}^{2+}/\text{SA}/\text{PAM}$ DN hydrogel, mainly due to the swelling of $\text{Ca}^{2+}/\text{SA}/\text{PAM}$ DN hydrogel and partial disintegration of the networks. However, the tensile strength and toughness of SA/PAM hydrogels

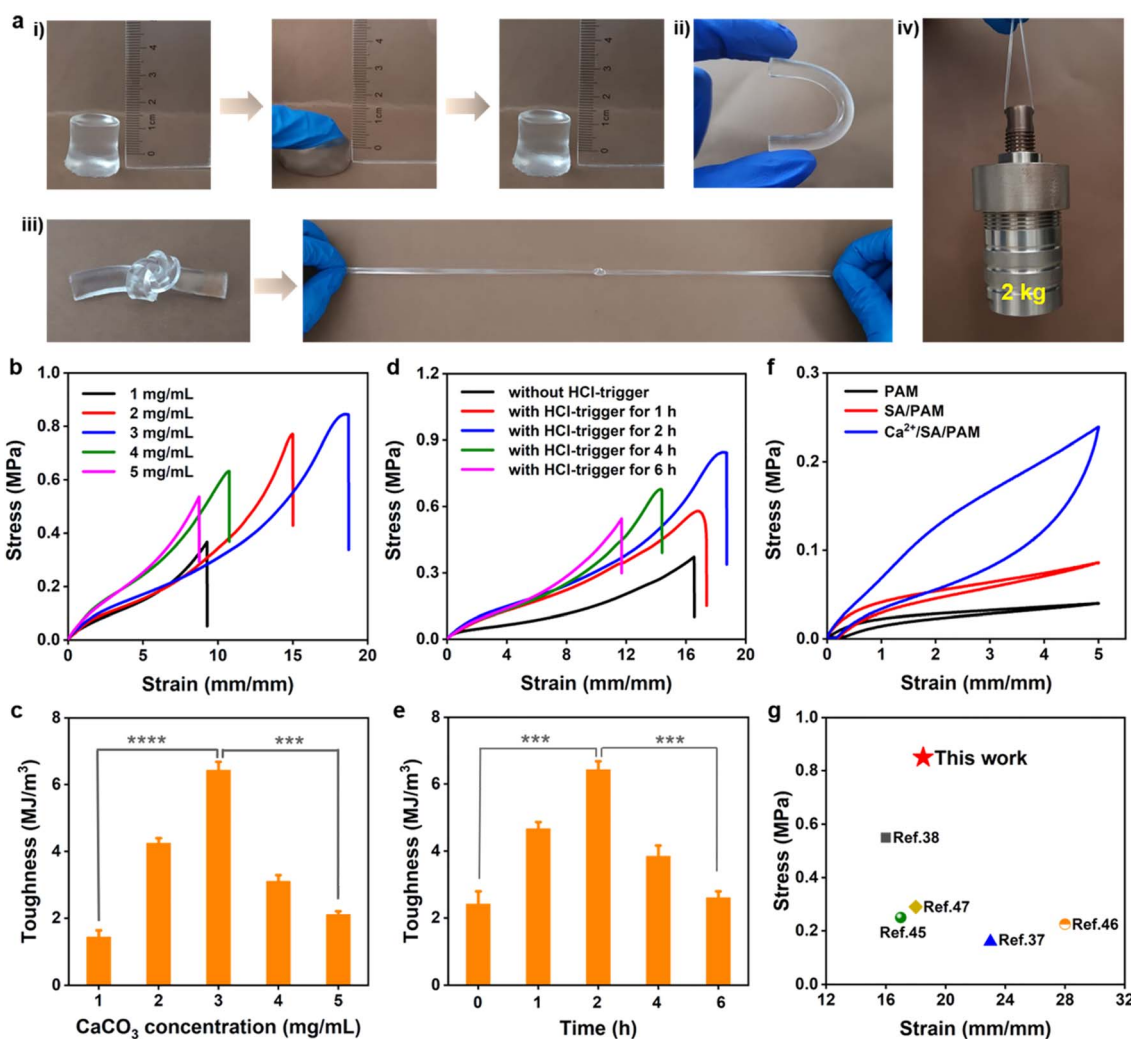


Fig. 2 (a) Demonstration of the deformation of $\text{Ca}^{2+}/\text{SA}/\text{PAM}$ DN hydrogels. (i) Compression, (ii) bending, (iii) knotting and stretching, and (iv) supporting a 2 kg weight. Tensile stress–strain curves and the corresponding toughness of $\text{Ca}^{2+}/\text{SA}/\text{PAM}$ DN hydrogels at (b and c) different CaCO_3 concentrations (incubation time of 2 h) or (d and e) different HCl incubation times (CaCO_3 concentration of 3 mg mL^{-1}). (f) Stress–strain curves by loading–unloading tests of PAM, SA/PAM, and $\text{Ca}^{2+}/\text{SA}/\text{PAM}$ DN hydrogels under 500% strain. (g) Comparison of the maximum strain and stress of $\text{Ca}^{2+}/\text{SA}/\text{PAM}$ DN hydrogels with those of typically reported hydrogels.

decreased from 0.27 to 0.15 MPa and 1.78 to 0.58 MJ m⁻³, respectively (Fig. S8†), when the incubation time increased to 6 h. This could be due to the absence of the ionic cross-linking networks and therefore the swelling of hydrogels under prolonged HCl incubation. Furthermore, the effect of the component (*i.e.*, SA, AM, and MBAA) concentrations was explored (Fig. S9–S11†). These results indicate that the mechanical properties of the hydrogels can be readily controlled *via* adjusting the concentrations of components. But importantly, the key parameter for increasing the tensile strength was the homogeneous incorporation of Ca²⁺ *via* the triggered dissolution of CaCO₃ microparticles, compared to the previously reported strategy of using CaSO₄ or CaCl₂ for the cross-linking of hydrogels (Fig. S12†).

To investigate the energy dissipation, hysteresis tensile tests at a fixed strain of 500% were conducted for PAM, SA/PAM, and Ca²⁺/SA/PAM DN hydrogels (Fig. 2f and S13†). The dissipative energies of PAM and SA/PAM hydrogels were 24.7 kJ m⁻³ and 37.9 kJ m⁻³, respectively, while the hysteresis loop of the Ca²⁺/SA/PAM DN hydrogel was about 12 times higher than that of the PAM hydrogel (293 kJ m⁻³). Subsequently, the elasticity and recovery properties of the Ca²⁺/SA/PAM DN hydrogels were examined by cyclic loading–unloading tensile tests (Fig. S14a†). The large hysteresis loop observed in the first loading–unloading cycle was due to the rearrangement of molecular chains and dynamic bonds in the Ca²⁺/SA/PAM DN hydrogel.⁴⁴ No breaking and apparent shifts were observed after ten loading–unloading cycles at a strain of 500%. The quantitative recovery and dissipated energy results showed that the recovery and dissipated energy were reduced after the first loading–unloading cycle but tended to remain unchanged in the next nine cycles. After ten loading–unloading cycles, the recovery ratio was still above 83% (Fig. S14b†), which indicated the good durability and anti-fatigue resistance properties of the Ca²⁺/SA/PAM DN hydrogels. The outstanding elasticity, recovery, and fatigue resistance of the hydrogels could be attributed to the synergy of the non-covalent cross-linking of the Ca²⁺/SA network and the covalent cross-linking of the PAM networks. Notably, the resulting Ca²⁺/SA/PAM DN hydrogels possessed three times higher tensile strength and strain than those of the existing Ca²⁺/SA/PAM-based hydrogels reported in the previous literature (Fig. 2g).^{37,38,45–47}

The performance of hydrogels under compression is another key factor governing their applications (*e.g.*, cartilage replacement, pressure sensor, *etc.*). Increasing the concentration of CaCO₃ microparticles resulted in an increase in compression strength and toughness, which could be tuned up to 8.5 MPa and 740 kJ m⁻³, respectively (Fig. S15†). The Ca²⁺/SA/PAM DN hydrogel was not fractured under 95% compression strain and could recover after 10 successive cycles of compressive deformations at 90% strain compression (Fig. S16a†). Although there was a slight decrease in the hysteresis loops at the end of the first cycle, curves from the subsequent cycles overlapped, which shows excellent resilience under compression. The slight decrease in the recovery ratio during continuous compressive–relaxation cycles also demonstrated the excellent shape-

recovery properties, outstanding elasticity, and good mechanical stability of the Ca²⁺/SA/PAM DN hydrogels (Fig. S16b†).

2.3 Electrical properties of Ca²⁺/SA/PAM DN hydrogels

Due to the high water content (80%) and porous nanostructures of hydrogels, high mobility of ions is typically present in the hydrogel matrix, thus leading to excellent ion conductivity. A light-emitting diode (LED) can be lit up in a circuit using the Ca²⁺/SA/PAM DN hydrogel as a conductor, and the brightness could be tuned by stretching or compressing the hydrogel (Fig. 3a and b). The LED brightness gradually became weak when the strain of the conductive hydrogel was between 0% and 600%, due to the increased ion transmission pathway; in contrast, the compression of the Ca²⁺/SA/PAM DN hydrogel could result in enhanced brightness, both of which confirmed its capability to monitor variations in strain and pressure. Moreover, the conductivity of hydrogels showed dependence on the different constitutions (Fig. 3c). Given the presence of ions, Ca²⁺/SA/PAM DN hydrogel exhibited an ionic conductivity of 0.85 S m⁻¹, which was about 2.8 times higher than that of PAM hydrogels (0.3 S m⁻¹).

The sensitivity of the Ca²⁺/SA/PAM DN hydrogels against tensile deformation was further investigated by measuring the change in the relative resistance ($\Delta R/R_0$) under different tensile strains (Fig. 3d). The GF, which represents the sensitivity of hydrogels, was calculated from the relative resistance change–strain curve and used to evaluate the electrical sensitivity. The curve can be roughly divided into three linear regions with GF values of 2.1 (0–200%), 5.5 (200–800%), and 8.9 (800–1800%), respectively, which were superior to those of most of the reported ionic conductive hydrogels.^{10,48–51} In addition, after 500 cycles of continuous loading–unloading tests with 50% strain, the sensor exhibited remarkable stability and prominent reproducibility with a negligible decay in the electrical signals (Fig. 3e). Benefitting from the elastic nature of the Ca²⁺/SA/PAM DN hydrogel, negligible hysteresis was observed during the tensile loading–unloading processes. Furthermore, the hydrogel showed high sensitivity in a wide range of strains. In the cyclic tensile test from 0.03% to 1500%, the Ca²⁺/SA/PAM DN hydrogel sensor was stretched five times at each strain and similar curves of resistance changes ($\Delta R/R_0$) were observed (Fig. 3f–h), suggesting good repeatability in the whole strain range. In comparison with the reported conductive hydrogels, Ca²⁺/SA/PAM DN hydrogel exhibited excellent mechanical and electrical properties over a wide range of sensitivity (Table S1†). Considering the superior stretchability, fatigue resistance, and electrical performances, the Ca²⁺/SA/PAM DN hydrogel is promising to be applied in the construction of wearable devices.

2.4 Human motion sensing

The biocompatibility of the obtained hydrogels was examined by a 3-(4,5-dimethylthiazol-2-yl)-2,5-diphenyltetrazolium bromide (MTT) assay and live/dead cell imaging after incubation with hydrogel extracts. As a result, cell viability was all above 99% after incubation of NIH-3T3 cells with hydrogel extracts for 24 h (Fig. S17†). The live/dead cell assay showed few dead cells

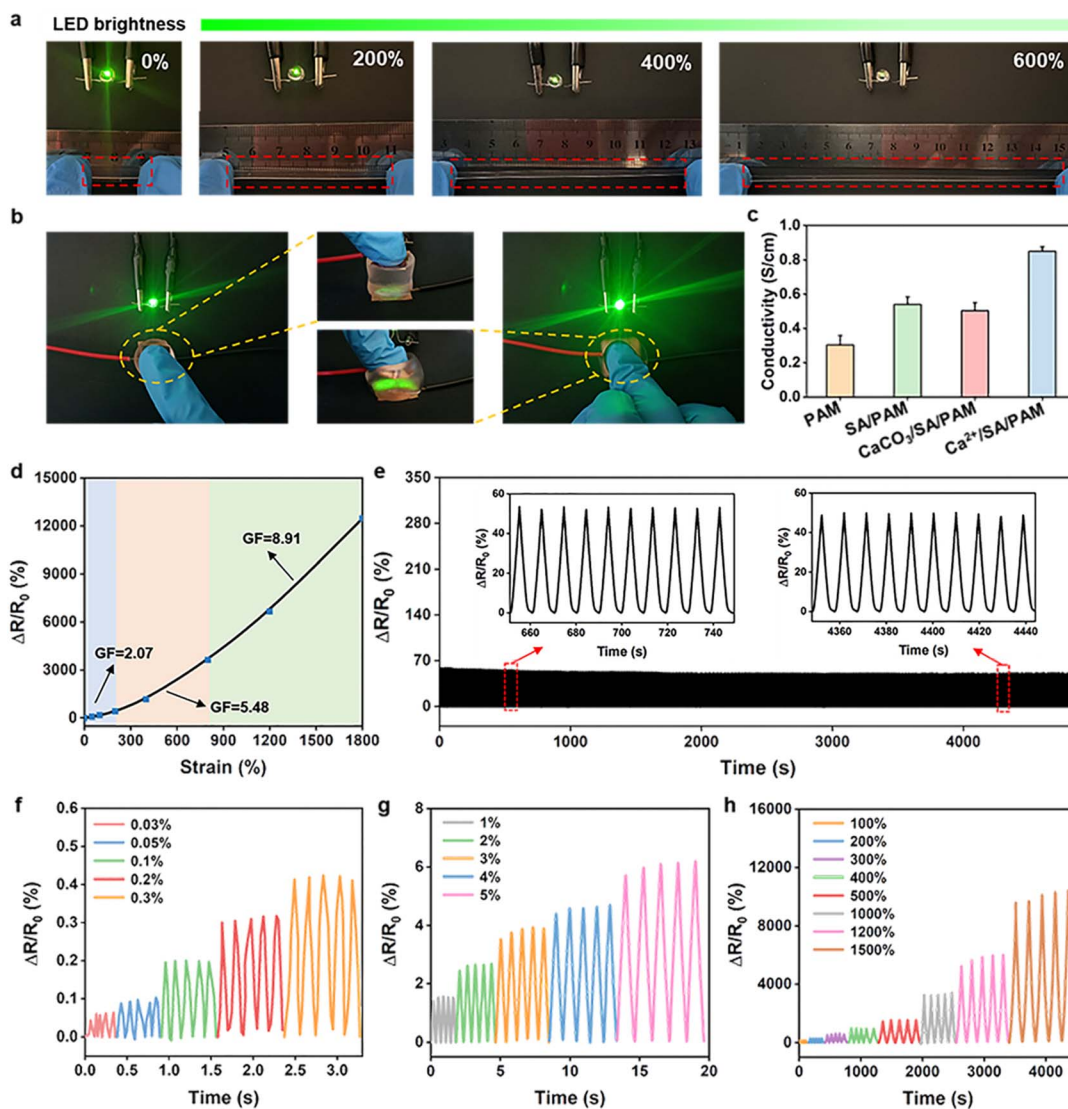


Fig. 3 Electromechanical characterization of the Ca²⁺/SA/PAM DN hydrogels. (a and b) Photographs showing the brightness of a LED lamp when Ca²⁺/SA/PAM DN hydrogel was under (a) stretching or (b) compression. (c) Conductivity of hydrogels with different compositions. (d) Relative electrical resistance change as a function of tensile strain for the Ca²⁺/SA/PAM DN hydrogel. (e) Relative resistance response during repeated loading–unloading processes with a strain of 50% for 500 cycles. (f–h) Relative resistance changes at different loading–unloading cycles under (f) small strains (0.03, 0.05, 0.1, 0.2, and 0.3%), (g) medium strains (1, 2, 3, 4, and 5%) and (h) large strains (100, 200, 300, 400, 500%, 1000%, 1200%, and 1500%).

after incubation with hydrogel extracts (Fig. S18†), which further confirmed the MTT results. These results indicated that the obtained hydrogels were biocompatible. To study the potential applications as a wearable strain sensor, Ca²⁺/SA/PAM DN hydrogel strips were mounted on diverse parts of the human body to monitor human activities (Fig. 4a). The relative resistance of the strain sensor increased as the finger bent stepwise from the straightened state to 120° (Fig. 4b), which was caused by the stretching of the hydrogel during finger movement. Furthermore, the relative resistance changes of the hydrogel could be recovered when the finger was re-straightened, indicating the high sensitivity of the hydrogel as a strain sensor. Specifically, the strain sensor of the Ca²⁺/SA/PAM DN hydrogel could feed back standing and sitting motions, when it was

adhered tightly to the knee (Fig. 4c). Similarly, the bending motions of the elbow and wrist (Fig. S19†) could also be monitored.

Taking advantage of the excellent sensitivity of tensile strain, the hydrogel sensor was further exploited to discern subtle human motions. Besides, facial expression recognition was readily realized, when the tester made expressions such as frowning (Fig. 4d). The corresponding relative resistance varied as a result of the compression and stretching of the hydrogel sensor, indicating the high sensitivity of the hydrogel device. This sensitivity is also reflected in facial inflating monitoring (Fig. 4e). When the Ca²⁺/SA/PAM DN hydrogel sensor was attached to the throat (Fig. 4f), the pressure caused by swallowing induced electrical variations that could also clearly be

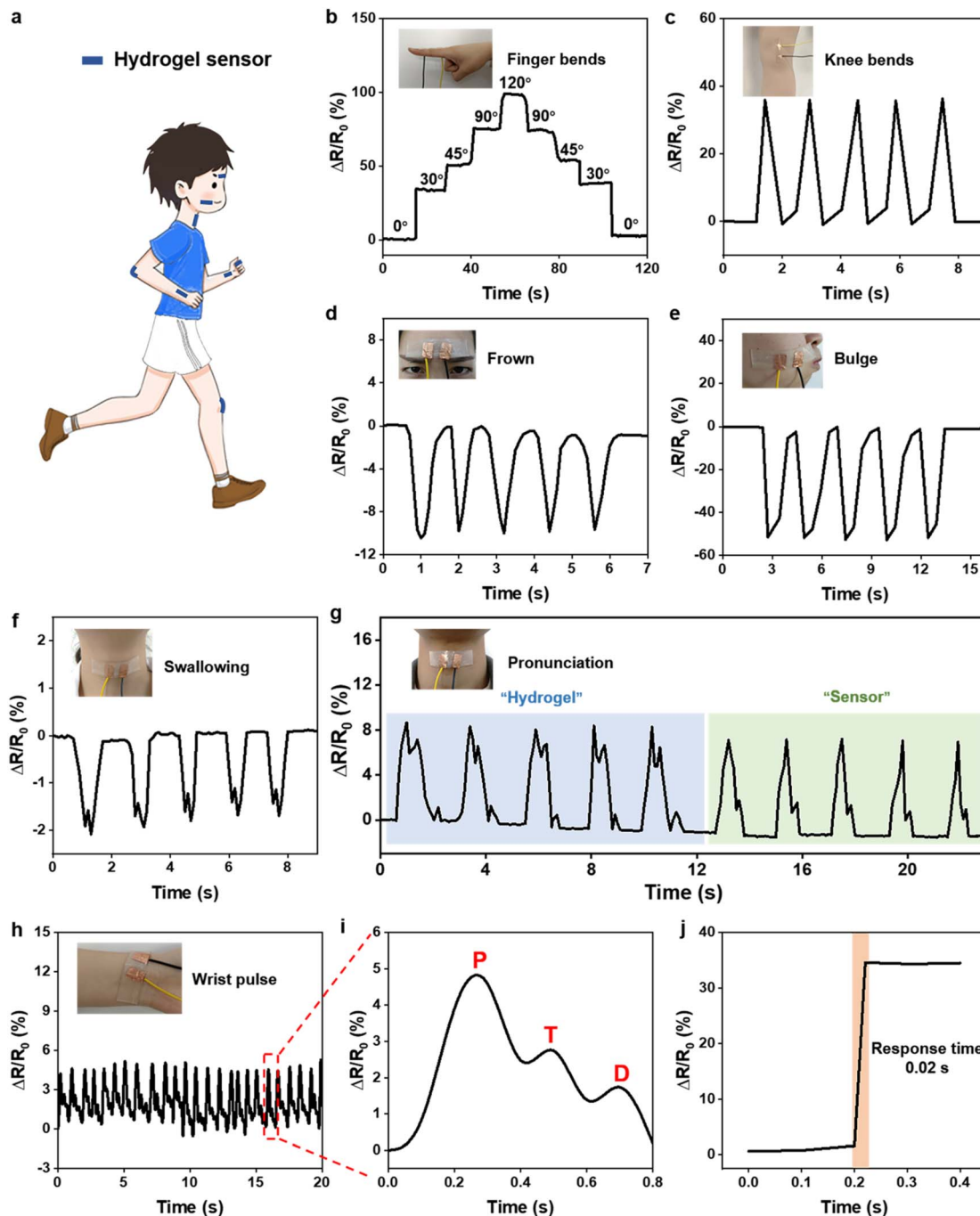


Fig. 4 Real-time monitoring of human motions by using a strain sensor prepared using $\text{Ca}^{2+}/\text{SA}/\text{PAM}$ DN hydrogels. (a) Schematic illustration of detecting human motions using the $\text{Ca}^{2+}/\text{SA}/\text{PAM}$ DN hydrogel sensor. (b–h) Signals of electrical resistance from (b) a finger at different bending angles, (c) knee joint, (d) making expressions of frowning, (e) inflating, (f) swallowing, (g) pronouncing different words, and (h) detecting the wrist pulse. (i) Waveform of a single pulse. (j) Response time of the $\text{Ca}^{2+}/\text{SA}/\text{PAM}$ DN hydrogel sensor.

distinguished. In addition, the muscle movements caused by speaking at the throat area can also be recorded accordingly (Fig. 4g). The time-dependent resistance curves could be recognized when the tester pronounced different words such as “hydrogel” and “sensor”. Furthermore, the $\text{Ca}^{2+}/\text{SA}/\text{PAM}$ DN hydrogel sensor could be used for real-time tracking of the human pulse on the wrist (Fig. 4h). The pulse rate (75 beats per min) calculated through the variation peaks was well fitted the

heartbeat frequency obtained from a sphygmomanometer. More importantly, the high sensitivity enabled the hydrogel sensor to distinguish three featured peaks from waveforms, the percussion wave (P), tidal wave (T), and diastolic wave (D), which were related to the blood pressure in the arteries caused by the systolic and diastolic processes of the heart (Fig. 4i).^{49,52} In addition, the strain sensor could rapidly monitor and distinguish all of these actions with a response time of ~ 0.02 s

(Fig. 4j), which is promising for the application in artificial intelligence, human motion monitoring, health management, and other fields in real life.

2.5 Mouse motion sensing and cascade reaction monitoring

In addition to monitoring the physiological signals and sporting motions of the human body, the Ca^{2+} /SA/PAM DN hydrogel sensor was also investigated to monitor the changes in the visceral organ resistance in mice and mild pain signals induced by an *in situ* cascade reaction at the wound site on a diabetic rat model in real-time. The stable electrical signal with a regular output showed a steady heartbeat of mice (Fig. 5a). The electrical resistance changed periodically with the trembling of the leg when needle stimulation was applied to the leg (Fig. 5b). Noteworthy, the high sensitivity Ca^{2+} /SA/PAM DN hydrogel sensor has great capability in recognizing different stimulations. It can provide a precise, reliable, and quantitative electrical response when different levels of weak and strong stimulations are applied to the tail (Fig. 5c).

To further demonstrate the accurate monitoring capability of the Ca^{2+} /SA/PAM DN hydrogel sensor, nanoparticles (NPs) were integrated with hydrogels and utilized for detecting the mild pain caused by cascade reactions in diabetic wounds,

where reactive oxygen species (ROS) is reported to have an influence on the sense of pains.^{53,54} We have previously reported that the combination of glucose oxidase (GOx) and iron ions into the same carriers could generate ROS *via* triggering the cascade reactions in the presence of glucose.⁵⁵ Herein, mesoporous silica/GOx@ tannic acid/ Fe^{2+} (MS/GOx@TA/ Fe^{2+}) NPs were prepared and used as a microreactor (Fig. S20–S23†). To verify that MS/GOx@TA/ Fe^{2+} NPs produce $\cdot\text{OH}$ *via* the cascade reaction, methylene blue (MB), a dye that can be discoloured by $\cdot\text{OH}$, was selected as an indicator of $\cdot\text{OH}$ generation.⁵⁶ The absorbance at 660 nm decreased and the solution became shallow, which demonstrated the generation of $\cdot\text{OH}$ produced by the cascade reactions (Fig. S24†). As illustrated in Fig. 5d, to monitor the pain signals, the hydrogel sensor was attached onto a diabetic wound, which was treated with MS/GOx@TA/ Fe^{2+} NPs to induce the cascade reactions due to the presence of glucose at the wound area. For the control of the hydrogel sensor or MS/GOx@TA/ Fe^{2+} NPs, the signal of electrical resistance tended to be a straight line. While using a Ca^{2+} /SA/PAM DN hydrogel sensor in combination with MS/GOx@TA/ Fe^{2+} NPs, the changes in electrical signals can be observed. The waveforms of electrical resistance were sharp in the beginning, but became wide with the extension of monitoring time probably due to the increasing amount of $\cdot\text{OH}$, which indicated the enhanced

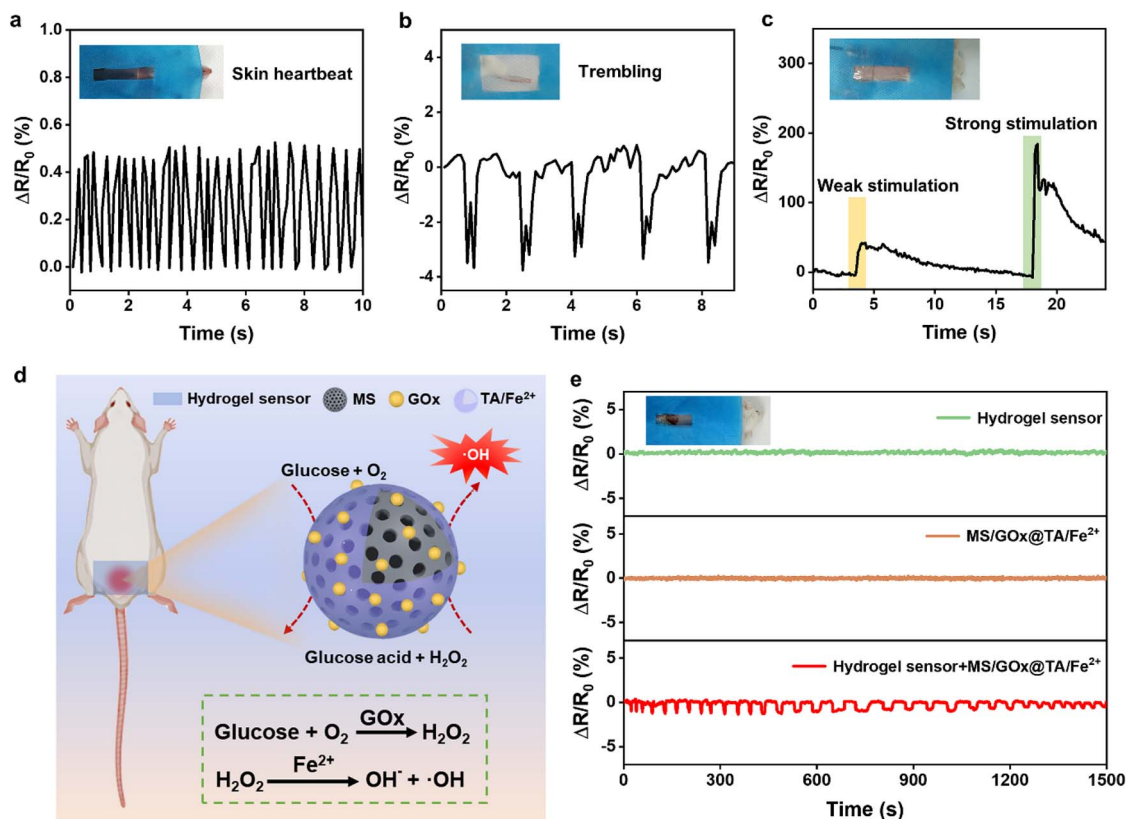


Fig. 5 Real-time monitoring of mouse motions. (a and b) The signals of electrical resistance from heartbeats and leg trembling. (c) Signals of electrical resistance from different levels of stimulation applied to the tail. (d) Schematic demonstration of *in situ* monitoring of pains caused by cascade reactions using a Ca^{2+} /SA/PAM DN hydrogel sensor in combination with MS/GOx@TA/ Fe^{2+} NPs. (e) Real-time resistance signals from the Ca^{2+} /SA/PAM DN hydrogel sensor, suspensions of MS/GOx@TA/ Fe^{2+} NPs, and the hydrogel sensor together with a MS/GOx@TA/ Fe^{2+} NP suspension.

degree of pain at the wound site. The waveforms became sharp again after ~20 min, which could be attributed to relief of the pain caused by the consumption of $\cdot\text{OH}$ (Fig. 5e). The monitoring performance of mild signals additionally evidenced the ultra-sensitive properties of the $\text{Ca}^{2+}/\text{SA}/\text{PAM}$ DN hydrogel.

3. Conclusions

In summary, a facile strategy for the preparation of $\text{Ca}^{2+}/\text{SA}/\text{PAM}$ DN hydrogels with strong and tough mechanical properties was established by pre-seeding CaCO_3 particles into a SA/PAM hydrogel, followed by the triggered release of Ca^{2+} from the microparticles for the cross-linking of SA . The mechanical properties of the hydrogels could be controlled by regulating the concentration of monomers and embedded CaCO_3 microparticles. The ionic bonds between Ca^{2+} and the carboxylate groups of SA were uniformly distributed within the $\text{Ca}^{2+}/\text{SA}/\text{PAM}$ DN hydrogels and served as the sacrificial bonds to efficiently dissipate the applied stress. The maximum tensile strength (0.85 MPa) and toughness (6.4 MJ m^{-3}) of the obtained hydrogels were significantly higher than those of previously reported SA/PAM hydrogels in the literature. Upon stretching for 500 cycles at 50% strain, the hydrogel sensor exhibited an excellent stability and durability. Electrical characterization evidenced the high sensitivity of the hydrogel in an extremely broad strain window (0.03–1800%), which granted the hydrogel applications in detecting human and mouse activities as a flexible sensor. Furthermore, the $\text{Ca}^{2+}/\text{SA}/\text{PAM}$ DN hydrogel sensor can also monitor *in situ* mild pains caused by a cascade reaction. The reported approach provides a new avenue for the fabrication of strong, tough, and moldable DN hydrogels with promise in the engineering of wearable sensors.

4. Experimental section

4.1 Reagents and materials

SA ($G/M = 2:1$) was purchased from Qingdao Hyzlin Biology Development Co., Ltd. (China). AM (99%), MBAA , TEMED , PAH and (3-aminopropyl)triethoxysilane (APTES) were bought from Shanghai Aladdin Biochemical Technology Co., Ltd. (China). Tetraethyl orthosilicate (TEOS), triethanolamine (TEOA), cetyltrimethylammonium tosylate (CTAT), TA , GOx , N -hydroxysuccinimide (NHS), calcein- AM , and propidium iodide (PI) were bought from Sigma-Aldrich (China). Ferrous glycinate ($\text{Fe}[\text{Gly}]_2$) was purchased from Macklin (China). N -(3-Dimethylaminopropyl)- N' -ethylcarbodiimide hydrochloride (EDC) and FITC were obtained from J&K Technology (China). APS , glucose, sodium phosphate dibasic dodecahydrate ($\text{Na}_2\text{HPO}_4 \cdot 12\text{H}_2\text{O}$), citric acid monohydrate, HCl solution (37%), acetone and ethanol were provided by Sinopharm Chemical Reagent Co., Ltd. (China). Streptomycin (STZ), Dulbecco's phosphate-buffered saline (DPBS) and MTT were purchased from Solarbio Biological Technology Co., Ltd. (China). Dulbecco's modified Eagle's medium (DMEM), antibiotic agents (penicillin/streptomycin, PS) and trypsin- EDTA solution were supplied by Biological Industries Science & Technology Co. Ltd. (China). Fetal bovine serum (FBS) was obtained from Gibco (USA). Water

with a resistivity of $18.2 \text{ M}\Omega \text{ cm}$ was prepared using a Milli-Q ultrapure water apparatus (Integral 5).

4.2 Preparation of CaCO_3 microparticles

CaCO_3 microparticles were prepared according to the method reported in the literature.^{57,58} Briefly, 10 mL of calcium chloride solution (0.33 M) and 10 mL of sodium carbonate solution (0.33 M) were quickly mixed and stirred vigorously for 30 s, followed by standing for 10 min. The precipitate was filtered and washed with water and acetone, followed by air-drying to obtain CaCO_3 microparticles. In order to obtain fluorescence-labeled CaCO_3 microparticles, the CaCO_3 microparticles were suspended in aqueous solution of FITC-PAH with a concentration of 2 mg mL^{-1} . After incubation for 1 h, the microparticles were washed three times with water to remove the unabsorbed FITC-PAH .

4.3 Preparation of the $\text{Ca}^{2+}/\text{SA}/\text{PAM}$ DN hydrogel

SA solution was prepared by dissolving SA powder in water at $25 \text{ }^\circ\text{C}$ under vigorous stirring for 4 h and then heated in a $50 \text{ }^\circ\text{C}$ water bath for 30 min until a transparent solution was obtained. Subsequently, AM and CaCO_3 microparticles were added to the SA precursor solution and stirred for 2 h. MBAA , APS , and TEMED were then added to the above solution and stirred for 10 min in an ice bath. The precursor solution was injected into a polytetrafluoroethylene plate mold (length \times width \times thickness = $150.0 \times 5.0 \times 2.0 \text{ mm}$) and 24-well cell culture plate. The samples were placed at $50 \text{ }^\circ\text{C}$ for 3 h to obtain the composite hydrogels. After thermo-polymerization, the obtained hydrogels were removed from the mold and soaked in HCl solution ($\text{pH} = 2$) at different time intervals. Finally, the obtained $\text{Ca}^{2+}/\text{SA}/\text{PAM}$ DN hydrogels were used for mechanical and other tests.

4.4 Characterization

The presence of CaCO_3 microparticles was verified by using CLSM (Leica TCP SP8 STED 3X, Germany). The morphologies of the hydrogels were characterized by SEM (Carl Zeiss G300, Germany). Before imaging, the cross section of the freeze-dried hydrogel sample was sputter-coated with gold. FTIR spectra were recorded in the range of $4000\text{--}750 \text{ cm}^{-1}$ using a Bruker Tensor II spectrometer (Germany). Morphologies of MS and $\text{MS}/\text{GOx}@\text{TA}/\text{Fe}^{2+}$ NPs were characterized by transmission electron microscopy (TEM , JEOL JEM-1400, Japan). The zeta potential of NPs was examined using a Zetasizer instrument (Malvern Panalytical, Zetasizer Pro, UK). UV-visible (UV-vis) absorption spectra were obtained on a Shimadzu UV-vis spectrophotometer (UV-2600, Japan).

4.5 Mechanical tests

The tensile and compression tests were performed with an Instron 3344 mechanical testing machine equipped with a 500 N load cell for tension and a 2000 N load cell for compression. The specimens with a rectangular shape ($50 \times 5 \times 2 \text{ mm}$) were subjected to tensile testing with a loading rate of 100 mm min^{-1} . The cylindrical samples with a diameter of 15 mm and a height of 12 mm were used for compression tests

with a rate of 5 mm min⁻¹. The nominal stress (σ) was obtained by dividing the force (F) by the cross-sectional area and the nominal tensile strain (ϵ) was obtained by dividing the stretched length (Δl) by the original length (l_0). The elastic modulus was calculated from the slope over 10–30% of the strain ratio of stress–strain curves. Compression stress was measured as F/A_0 , where F is the force and A_0 is original cross-section area. Compression strain was estimated as h/h_0 , where h and h_0 are the deformed height and original height, respectively. The toughness of hydrogels was simply calculated as the area under the stress–strain curves. The rates of the tensile loading–unloading test and compression–relaxation test were fixed at 100 and 5 mm min⁻¹, respectively, without any detention time.

4.6 Water absorption tests

To investigate the water absorption ratio of PAM, SA/PAM, and Ca²⁺/SA/PAM DN hydrogels, hydrogels were freeze-dried and weighed to obtain the mass of polymer networks. The dried polymer networks were immersed in water until the swelling was equilibrated. The swollen hydrogels were weighed after removing the excess water using a filter paper at different time points. The water absorption ratio (R) was calculated as below:

$$R = (W_s - W_d)/W_d$$

where W_s and W_d are the weights of the swollen and dried hydrogels, respectively.

4.7 Electrical and sensing performances of hydrogels

The conductivity of hydrogels was measured using an electrochemical workstation (Princeton VersaSTAT4, USA). The conductivity was calculated according to the following equation:

$$\sigma = L/(R \times S)$$

where σ , L , S , and R represent ionic conductivity, height of the gel, cross-section area of the hydrogel, and the measured resistance value, respectively.

The sensing properties of the Ca²⁺/SA/PAM DN hydrogels were investigated by combined manipulations of a mechanical testing machine (Instron 3344, USA) and digital meter (Keithley 2614B, USA) to record the real-time resistance and strain. The relative changes in resistance were calculated using the formula:

$$\Delta R/R_0 = (R - R_0)/R_0$$

where R_0 and R represent the initial resistance and the real-time resistance, respectively.

The sensitivity of the hydrogel strain sensor is characterized by the GF using the following formula:

$$GF = \Delta R/R_0/\epsilon$$

where ϵ is the applied strain.

4.8 Strain sensor fabrication and electrical tests

A strain sensor was assembled by using the Ca²⁺/SA/PAM DN hydrogel as a conductor and VHB tape as the elastomeric substrate and an encapsulant. The top and bottom of the sensor were insulated using the VHB tape to prevent water evaporation from the hydrogel. For human and mouse motion detection, the real-time electrical signals of the strain sensors based on the resistance changes in a different state were recorded by a digital meter (Keithley 2614B, USA). The relative changes in the resistance were calculated based on the monitored current:

$$\Delta R/R_0 = (R_s - R_0)/R_0$$

where R_0 and R_s are the resistances without and with applied strain, respectively.

4.9 In vitro biocompatibility test of hydrogels

The biocompatibility of hydrogels was examined by using an MTT assay and live/dead cell imaging. Briefly, hydrogels were incubated in a DMEM medium for 24 h at 37 °C (20 mg of hydrogels per mL of medium) and the supernatant (hydrogel extract) was filtered using 0.22 μ m filters. NIH-3T3 mouse fibroblast cells (1×10^4 cells per mL) were seeded in a 96-well plate and cultured in DMEM complete medium for 12 h. Subsequently, the culture media were removed, followed by the addition of 100 μ L of the hydrogel extract. After 24 h of incubation, the cell viability was quantified by an MTT assay. The absorbance at 490 nm was recorded using a microplate reader (TECAN Spark 10M, Austria). Additionally, cells were stained with calcein-AM/PI and imaged using an inverted fluorescence microscope (Leica DMI8, Germany).

4.10 Preparation of MS NPs

MS NPs were prepared by using a previously reported method.⁵⁹ Briefly, CTAT (0.96 g) and TEOA (174 mg) were dissolved in 50 mL of water and the solution was stirred at 80 °C for 1 h before TEOS (7.29 g) was added. After stirring for another 2 h, the resultant NPs were washed with water and ethanol three times, followed by calcination at 550 °C for 6 h to obtain MS NPs.

4.11 Preparation of MS/GOx@TA/Fe²⁺ NPs

GOx was loaded into MS NPs according to a literature method.⁶⁰ In brief, EDC (30 mg), NHS (47.5 mg) and GOx (4 mg) were dissolved in 5 mL of water, followed by the addition of 37 μ L APTES. The mixture was stirred for 8 h to produce amino-functionalized GOx. Subsequently, MS (16.7 mg) was added to the mixture and stirred for 24 h. The MS/GOx NPs were washed with water three times and obtained by centrifugation (13 000 rcf 10 min).

Fe[Gly]₂ solution (2 mg mL⁻¹, 250 μ L) and TA solution (40 mg mL⁻¹, 200 μ L) were mixed vigorously for 10 s before adding into the suspension of MS/GOx NPs. After stirring for 2 min, MS/GOx@TA/Fe²⁺ NPs were washed with water three times and obtained by centrifugation (13 000 rcf 10 min).

4.12 Detection of 'OH generation

MB solution (25 $\mu\text{g mL}^{-1}$, 800 μL), glucose solution (5 mg mL^{-1} , 400 μL), MS/GOx@TA/Fe²⁺ NPs suspension (400 μL) and citric acid–disodium hydrogen phosphate buffer solution (pH 4.5, 1.4 mL) were mixed together and incubated for different time periods. The UV-vis absorption of the mixture solution was measured.

4.13 *In situ* monitoring of mild pains caused by cascade reactions

Animal ethics were approved by Shandong University according to the Health Guide for the Care and Use of Laboratory Animals of National Institutes. SD rats were obtained from Vital River Laboratory Animal Technology (China). Fifteen rats were randomly divided into three groups ($n = 5$), including Ca²⁺/SA/PAM DN hydrogels (hydrogel sensor), MS/GOx@TA/Fe²⁺ NPs, and hydrogel sensor + MS/GOx@TA/Fe²⁺ NPs. To establish a diabetic rat model, the rats were administered with a daily dose of 60 μg per g body weight streptozotocin *via* intravenous injection until the fasting blood sugar rose to >16.7 mM. Upon anesthetization, a 1 cm-diameter wound was generated on each rat and 100 μL of MS/GOx@TA/Fe²⁺ suspension was introduced to the wound sites. Subsequently, the Ca²⁺/SA/PAM hydrogel sensor was attached to the wound site to monitor mild pain signals caused by the cascade reaction. The rats were euthanized after the experiments and disposed of according to the Health Guide for the Care and Use of Laboratory Animals of National Institutes.

Conflicts of interest

The authors declare that they have no competing financial interests or personal relationships that could have appeared to influence the work reported in this paper.

Acknowledgements

This research was supported by the National Natural Science Foundation of China (22202119 and 21872085) and the Innovation Project of Jinan Science and Technology Bureau (2020GXRC022). This work was performed in part at the Analytical Centre for Structural Constituent and Physical Property, and the Translational Medicine Core Facility of Advanced Medical Research Institute at Shandong University.

References

- Q.-F. Guan, H.-B. Yang, Z.-M. Han, Z.-C. Ling, C.-H. Yin, K.-P. Yang, Y.-X. Zhao and S.-H. Yu, *ACS Nano*, 2021, **15**, 7889–7898.
- E. Nicol, *Biomacromolecules*, 2021, **22**, 1325–1345.
- H. Geng, Q. Dai, H. Sun, L. Zhuang, A. Song, F. Caruso, J. Hao and J. Cui, *ACS Appl. Bio Mater.*, 2020, **3**, 1258–1266.
- C.-H. Lu, C.-H. Yu and Y.-C. Yeh, *Acta Biomater.*, 2021, **130**, 66–79.
- X. Ding, H. Zhao, Y. Li, A. L. Lee, Z. Li, M. Fu, C. Li, Y. Y. Yang and P. Yuan, *Adv. Drug Delivery Rev.*, 2020, **160**, 78–104.
- T. Su, M. Zhang, Q. Zeng, W. Pan, Y. Huang, Y. Qian, W. Dong, X. Qi and J. Shen, *Bioact. Mater.*, 2021, **6**, 579–588.
- Y. Wang, S. Zhang and J. Wang, *Chin. Chem. Lett.*, 2021, **32**, 1603–1614.
- H. Zheng, N. Lin, Y. He and B. Zuo, *ACS Appl. Mater. Interfaces*, 2021, **13**, 40013–40031.
- H. Qiao, P. Qi, X. Zhang, L. Wang, Y. Tan, Z. Luan, Y. Xia, Y. Li and K. Sui, *ACS Appl. Mater. Interfaces*, 2019, **11**, 7755–7763.
- X. Zhang, N. Sheng, L. Wang, Y. Tan, C. Liu, Y. Xia, Z. Nie and K. Sui, *Mater. Horiz.*, 2019, **6**, 326–333.
- J. Xu, R. Jing, X. Ren and G. Gao, *J. Mater. Chem. A*, 2020, **8**, 9373–9381.
- S.-L. Xiang, Y.-X. Su, H. Yin, C. Li and M.-Q. Zhu, *Nano Energy*, 2021, **85**, 105965.
- H. Cui, N. Pan, W. Fan, C. Liu, Y. Li, Y. Xia and K. Sui, *Adv. Funct. Mater.*, 2019, **29**, 1807692.
- M. Li, X. Wang, B. Dong and M. Sitti, *Nat. Commun.*, 2020, **11**, 3988.
- Z. Shen, X. Zhu, C. Majidi and G. Gu, *Adv. Mater.*, 2021, **33**, 2102069.
- L.-Y. Hsiao, L. Jing, K. Li, H. Yang, Y. Li and P.-Y. Chen, *Carbon*, 2020, **161**, 784–793.
- D. Han, C. Farino, C. Yang, T. Scott, D. Browe, W. Choi, J. W. Freeman and H. Lee, *ACS Appl. Mater. Interfaces*, 2018, **10**, 17512–17518.
- S. Wu, Z. Shao, H. Xie, T. Xiang and S. Zhou, *J. Mater. Chem. A*, 2021, **9**, 1048–1061.
- Q. Pang, D. Lou, S. Li, G. Wang, B. Qiao, S. Dong, L. Ma, C. Gao and Z. Wu, *Adv. Sci.*, 2020, **7**, 1902673.
- Y. Wang, Y. Yu, J. Guo, Z. Zhang, X. Zhang and Y. Zhao, *Adv. Funct. Mater.*, 2020, **30**, 2000151.
- X. Sui, H. Guo, P. Chen, Y. Zhu, C. Wen, Y. Gao, J. Yang, X. Zhang and L. Zhang, *Adv. Funct. Mater.*, 2019, **30**, 1907986.
- J. Chen, X. Xu, M. Liu, Y. Li, D. Yu, Y. Lu, M. Xiong, I. Wyman, X. Xu and X. Wu, *Carbohydr. Polym.*, 2021, **264**, 117978.
- W. Yuan, Z. Li, X. Xie, Z. Y. Zhang and L. Bian, *Bioact. Mater.*, 2020, **5**, 819–831.
- C. Teng, D. Xie, J. Wang, Y. Zhu and L. Jiang, *J. Mater. Chem. A*, 2016, **4**, 12884–12888.
- B. Sui, Y. Li and B. Yang, *Chin. Chem. Lett.*, 2020, **31**, 1443–1447.
- T. Huang, H. Xu, K. Jiao, P. Zhu, H. R. Brown and H. Wang, *Adv. Mater.*, 2007, **19**, 1622–1626.
- H. Sun, Y. Zhao, C. Wang, K. Zhou, C. Yan, G. Zheng, J. Huang, K. Dai, C. Liu and C. Shen, *Nano Energy*, 2020, **76**, 105035.
- Y. Zhang, Q. Hu, S. Yang, T. Wang, W. Sun and Z. Tong, *Macromolecules*, 2021, **54**, 5218–5228.
- H. C. Yu, S. Y. Zheng, L. Fang, Z. Ying, M. Du, J. Wang, K. F. Ren, Z. L. Wu and Q. Zheng, *Adv. Mater.*, 2020, **32**, 2005171.
- Y. Huang, L. Xiao, J. Zhou, T. Liu, Y. Yan, S. Long and X. Li, *Adv. Funct. Mater.*, 2021, **31**, 2103917.

- 31 J. P. Gong, Y. Katsuyama, T. Kurokawa and Y. Osada, *Adv. Mater.*, 2003, **15**, 1155–1158.
- 32 Y. Yang, X. Wang, F. Yang, L. Wang and D. Wu, *Adv. Mater.*, 2018, **30**, 1707071.
- 33 G. Liu, C. Zhou, W. L. Teo, C. Qian and Y. Zhao, *Angew. Chem., Int. Ed.*, 2019, **58**, 9366–9372.
- 34 W. Tanaka, H. Shigemitsu, T. Fujisaku, R. Kubota, S. Minami, K. Urayama and I. Hamachi, *J. Am. Chem. Soc.*, 2019, **141**, 4997–5004.
- 35 Q. Chen, H. Chen, L. Zhu and J. Zheng, *Macromol. Chem. Phys.*, 2016, **217**, 1022–1036.
- 36 Q. Zheng, L. Zhao, J. Wang, S. Wang, Y. Liu and X. Liu, *Colloids Surf., A*, 2020, **589**, 124402.
- 37 J. Y. Sun, X. Zhao, W. R. Illeperuma, O. Chaudhuri, K. H. Oh, D. J. Mooney, J. J. Vlassak and Z. Suo, *Nature*, 2012, **489**, 133–136.
- 38 C. H. Yang, M. X. Wang, H. Haider, J. H. Yang, J. Y. Sun, Y. M. Chen, J. Zhou and Z. Suo, *ACS Appl. Mater. Interfaces*, 2013, **5**, 10418–10422.
- 39 X.-Y. Liu, H. Xu, L.-Q. Zhang, M. Zhong and X.-M. Xie, *ACS Appl. Mater. Interfaces*, 2019, **11**, 42856–42864.
- 40 C. Li, X. Zhou, D. Zhou, F. Chen, J. Shen, H. Li, J. Zhang and X. Zhou, *ACS Appl. Polym. Mater.*, 2019, **1**, 3222–3226.
- 41 S. Hua, H. Ma, X. Li, H. Yang and A. Wang, *Int. J. Biol. Macromol.*, 2010, **46**, 517–523.
- 42 J. Liu, Q. Zhang, Z.-Y. Wu, J.-H. Wu, J.-T. Li, L. Huang and S.-G. Sun, *Chem. Commun.*, 2014, **50**, 6386–6389.
- 43 A. Saari, V. Kasparkova, T. Sedlacek and P. Saha, *J. Mech. Behav. Biomed. Mater.*, 2013, **18**, 152–166.
- 44 Y. Wei, L. Xiang, H. Ou, F. Li, Y. Zhang, Y. Qian, L. Hao, J. Diao, M. Zhang, P. Zhu, Y. Liu, Y. Kuang and G. Chen, *Adv. Funct. Mater.*, 2020, **30**, 2005135.
- 45 J. Li, W. R. K. Illeperuma, Z. Suo and J. J. Vlassak, *ACS Macro Lett.*, 2014, **3**, 520–523.
- 46 J. Chen, L. Zhang, Y. Tu, Q. Zhang, F. Peng, W. Zeng, M. Zhang and X. Tao, *Nano Energy*, 2021, **88**, 106272.
- 47 C. Li, X. Zhou, D. Zhou, F. Chen, J. Shen, H. Li, J. Zhang and X. Zhou, *ACS Appl. Polym. Mater.*, 2019, **1**, 3222–3226.
- 48 J. Yu, Y. Feng, D. Sun, W. Ren, C. Shao and R. Sun, *ACS Appl. Mater. Interfaces*, 2022, **14**, 10886–10897.
- 49 M. Wu, J. Chen, Y. Ma, B. Yan, M. Pan, Q. Peng, W. Wang, L. Han, J. Liu and H. Zeng, *J. Mater. Chem. A*, 2020, **8**, 24718–24733.
- 50 A. Wang, Y. Wang, B. Zhang, K. Wan, J. Zhu, J. Xu, C. Zhang and T. Liu, *Chem. Eng. J.*, 2021, **411**, 128506.
- 51 H. Wei, Z. Wang, H. Zhang, Y. Huang, Z. Wang, Y. Zhou, B. B. Xu, S. Halila and J. Chen, *Chem. Mater.*, 2021, **33**, 6731–6742.
- 52 Z. Yang, Y. Pang, X. L. Han, Y. Yang, J. Ling, M. Jian, Y. Zhang, Y. Yang and T. L. Ren, *ACS Nano*, 2018, **12**, 9134–9141.
- 53 D. Hackel, D. Pflucke, A. Neumann, J. Viebahn, S. Mousa, E. Wischmeyer, N. Roewer, A. Brack and H. L. Rittner, *PLoS One*, 2013, **8**, e63564.
- 54 J. Yowtak, K. Y. Lee, H. Y. Kim, J. Wang, H. K. Kim, K. Chung and J. M. Chung, *Pain*, 2011, **152**, 844–852.
- 55 Q. Wang, Z. Gao, Q.-Z. Zhong, N. Wang, H. Mei, Q. Dai, J. Cui and J. Hao, *Langmuir*, 2021, **37**, 11292–11300.
- 56 Y. Guo, H.-R. Jia, X. Zhang, X. Zhang, Q. Sun, S.-Z. Wang, J. Zhao and F.-G. Wu, *Small*, 2020, **16**, 2000897.
- 57 D. V. Volodkin, N. I. Larionova and G. B. Sukhorukov, *Biomacromolecules*, 2004, **5**, 1962–1972.
- 58 D. V. Volodkin, A. I. Petrov, M. Prevot and G. B. Sukhorukov, *Langmuir*, 2004, **20**, 3398–3406.
- 59 P. Zhang, Z. Gao, J. Cui and J. Hao, *ACS Appl. Bio Mater.*, 2020, **3**, 561–569.
- 60 M. Shi, Z. Du, Y. Qi, W. Li, H. Hu, X. Lin, S. Wang, Z. Tang and M. Zhou, *Theranostics*, 2022, **12**, 2658–2673.